

Analysis of Jet Effects on Co-Flow Jet Airfoil Performance with Integrated Propulsion System

Ge-Cheng Zha* and Wei Gao †
Dept. of Mechanical and Aerospace Engineering
University of Miami
Coral Gables, Florida 33124
E-mail: gzha@miami.edu

Abstract

A control volume analysis is given in this paper to analyze the jet effect on co-flow jet airfoil with injection and suction and the airfoil with injection only. The ducts reaction forces formulations to be included for lift and drag calculation are given. CFD solutions based on RANS model are used to provide the breakdowns of lift and drag contributions from the airfoil surface force integral and jet ducts reaction forces. The results are compared with experiment as validation. The duct reaction forces are also validated by a 3D CFD calculation of the complete airfoil with jet ducts and wind tunnel wall.

A comparative study of the jet effect on airfoil performance between the CFJ airfoil with injection and suction and the airfoil with injection only is conducted. The study indicates that the suction occurring on the airfoil suction surface such as the CFJ airfoil is more beneficial than the suction occurring through the engine inlet such as the airfoil with injection only. For the airfoil with injection only, the drag actually acted on the aircraft, the equivalent drag, could be significantly larger than the drag measured by the wind tunnel balance because of the ram and captured area drag when the jet is drawn from the freestream. For CFJ airfoil, the drag measured by the wind tunnel balance is the actual 2D drag that the aircraft will be experienced. The CFJ airfoil does not have the ram drag and captured area drag. For a CFJ airfoil, the suction penalty is offset by the significant circulation enhancement. The CFJ airfoil with both injection and suction yields stronger mixing, larger circulation, more filled wake, higher stall angle of attack, less drag, and more efficient energy expenditure.

* Associate Professor, AIAA Member

† Graduate Student

1 Nomenclature

A	Area
AoA	Angle of Attack
CFD	Computational Fluid Dynamics
CFJ	Co-Flow Jet
CC	Circulation Control
C_L	Lift Coefficient
C_D	drag Coefficient
C_μ	Momentum Coefficient
D	Drag
E	Endurance
F	Resultant Force
FC	Flow Control
\dot{m}	Mass Flow Rate
k	Turbulent Kinetic Energy
L	Lift
M	Mach Number
p	Static pressure
P	Power required
P_t	Total Pressure
R	Force from airfoil surface integral
R'	Reaction force of R
Re	Reynolds number
S	Wing Span Area ($b \times chord$)
u,v,w	Velocity components in x-, y-, and z-direction
V	Velocity vector
y^+	non-dimensional length scale for turbulent boundary layer

Subscripts:

e	control volume exit
ei	engine inlet
j	jet injection
∞	Freestream

Greek Letters:

ϵ	Turbulent Dissipation Rate
γ	Ratio of Specific Heats
ρ	Density
∞	Freestream
α	Angle of Attack
θ	Angle between slot surface and the line normal to chord

2 Introduction

Flow control (FC) is a promising means to significantly improve airfoil performance and has attracted more and more attention lately as the technology for future high performance high efficiency

aircraft[1, 2, 3, 4, 5, 6, 7]. Zha el al. have recently developed a new airfoil flow control technique using co-flow jet [8, 9, 10], which dramatically increases lift, stall margin, and drag reduction.

The co-flow jet airfoil is to open an injection slot near leading edge and a suction slot near trailing edge on the airfoil suction surface. A high energy jet is injected near leading edge tangentially and the same amount of mass flow is sucked in near trailing edge. The turbulent shear layer between the main flow and the jet causes strong turbulence diffusion and mixing under severe adverse pressure gradient, which enhances lateral transport of energy from the jet to mainflow and allows the main flow to overcome severe adverse pressure gradient and remain attached at high angle of attack(AoA). The high energy jet induces high circulation and hence generates high lift. The energized main flow fills the wake and therefore reduce drag. The CFJ airfoil can recirculate the jet mass flow to achieve zero net jet mass flow and minimize the penalty to propulsion system due to no dumped jet mass flow, as shown in the sketch of Fig.1.

In [11, 9], an overview of different flow control methods is given. Compared with the circulation control (CC) airfoil[12, 13] as shown in the sketch of Fig. 2, the working mechanism of CFJ airfoil is different. A CC airfoil relies on large leading edge(LE) or trailing edge (TE) to have the Coanda effect and enhance circulation. The large TE or LE hence are required, which may generate large drag during cruise. The CFJ airfoil relies on the wall jet mixing with the main flow to energize the main flow and overcome the adverse pressure gradient so that the flow can induce high circulation and remain attached at high AoA. The CC airfoil dumps away the jet mass flow, which is a considerable penalty to the propulsion system. The CFJ airfoil recirculates the jet mass flow and achieves the zero net jet mass flow to significantly reduce the penalty to propulsion system. A CC airfoil without LE injection will reduce stall margin even though it increase the lift[14]. Compared with the synthetic jet flow control, the enhancement of airfoil performance by the CFJ airfoil is much more dramatic because the interaction of the synthetic jet with the main flow is weak[11, 9, 15]. The synthetic jet airfoil also has little stall margin increase[15]. CFJ airfoil simultaneously achieves three dramatic effects at low energy expenditure: lift enhancement, stall margin increase, and drag reduction. The mission analysis conducted in [11] indicates a significant improvement of fuel consumption reduction, increase of range and endurance, and a dramatic reduction of take off and landing distance.

The turbulent mixing between the jet and main flow to transfer energy from the jet to the main flow is the fundamental working principle of CFJ airfoil [11]. The CFJ airfoil performance is more sensitive to the injection than to the suction. The injection slot should be located as close to the leading edge as possible, but should be located downstream of the suction peak. This is to make use of the adverse pressure gradient after the suction peak to enhance the wall jet mixing with the main flow[16]. In [9, 10], the injection slot size effect is studied experimentally. It is found that the smaller injection slot has higher stall AoA and hence high maximum lift. The energy expenditure of the airfoil with smaller injection slot is significantly less than that of the airfoil with large injection slot size. This indicates that there is a great potential to optimize the CFJ airfoil performance such as reducing the amount of jet mass flow with optimum configuration or pulsed jet, etc. What is important in the research of [11, 9, 10] is that the CFJ airfoil concept is proved to be effective.

The coflow jet airfoil concept suggested by Zha el al. [11, 9] appears to have the following advantages: 1) Very effective to enhance lift and suppress separation; 2) Dramatically reduce drag and can achieve very high C_L/C_D at low AoA(cruise), and very high lift and drag at high AoA(take off and landing); 3) Significantly increase AoA operating range and stall margin; 4) Have small penalty to the propulsion system; 5) Can be applied to any airfoil, thick or thin; 6) Can be used for whole flying mission instead of only take off and landing; 7) Can be used for low and high

speed aircraft; 8) Easy implementation with no moving parts;

The CFJ airfoil concept is new and hence many issues of the working mechanism need to be further studied. One question is: Compared with the CC airfoil which has no suction, will the streamwise suction of the CFJ airfoil hurt the airfoil performance? This question is based on the conception that a streamwise injection will generate a thrust due to its momentum and hence reduce the drag, a streamwise suction will do the opposite. However, any flow control process involved an injection must need a suction, which is the law of mass conservation, unless the jet is generated internally such as the rocket combustion. The question then becomes: where and how the suction occurs will be more beneficial, the suction occurring on the airfoil suction surface such as a CFJ airfoil (see Fig. 1) or the suction occurring on the engine such as a CC airfoil (see Fig.2)?

The objective of this paper is to conduct a control volume analysis to analyze the effect of the injection and suction jet. 2D and 3D CFD simulations are used to provide the detailed data breakdowns. The experimental results are used to validate the results. For the airfoil with injection only, the equivalent drag, which is the drag actually acted on the aircraft, could be significantly larger than the drag measured by the wind tunnel balance because of the ram and captured area drag when the jet is drawn from the freestream through the aircraft engine inlet. For a CFJ airfoil, the drag measured by the wind tunnel balance is the actual 2D drag that the aircraft will be experienced. The CFJ airfoil does not have the ram drag and captured area drag. The measured performance of the CFJ airfoil has already included the suction penalty, which is offset by the significant circulation enhancement. The CFJ airfoil with both injection and suction yields stronger mixing, larger circulation, more filled wake, higher stall angle of attack, less drag, and more efficient energy expenditure.

3 Control Volume Analysis

3.1 CFJ Airfoil

Take a control volume **abcdefghia** surrounding a CFJ airfoil as shown in Fig. 3 with the following assumptions: the freestream flow comes into the control volume from the inlet on the left and exits the control volume from the outlet on the right. The freestream flow is perpendicular to the inlet and outlet boundaries. The upper and lower boundaries are parallel to the freestream flow. The pressure at the inlet and outlet are uniform and are equal to the freestream pressure. A jet injects from slot 1 and the same amount of mass flow is drawn into the airfoil at slot 2. The flow is steady state inside the control volume.

Let \mathbf{R}_x and \mathbf{R}_y represent the components of the pressure and shear stress integral acted by the **airfoil surface** on the control volume in x and y directions.

The momentum equation on the control volume **abcdefghia** gives:

$$\sum \mathbf{F} = \int \int_s \rho \mathbf{V} \cdot d\mathbf{S} \cdot \mathbf{V} \quad (1)$$

The left side of above equation is the resultant force of the control volume. The right side of the equation is the momentum variation across the control volume boundary.

Eq. (1) in x-direction is:

$$-p_e A_e + p_\infty A_\infty + (p_{j1} A_{j1})_x - (p_{j2} A_{j2})_x + R_x = \int_h^b \rho V_e \cdot dy \cdot V_e - \int_i^a \rho V_\infty \cdot dy \cdot V_\infty - \dot{m}_{j1} u_{j1} + \dot{m}_{j2} u_{j2} \quad (2)$$

The subscripts 1 and 2 stand for the jet injection and suction. Since $p_e = p_\infty$ and $A_e = A_\infty$, the first two items on the left side of above equation are canceled out.

Let $F_{x_{cfj}}$ stand for the the reaction force generated by the jet ducts in x-direction, then

$$\begin{aligned} F_{x_{cfj}} &= (\dot{m}_{j1} u_{j1} + (p_{j1} A_{j1})_x) - \gamma(\dot{m}_{j2} u_{j2} + (p_{j2} A_{j2})_x) \\ &= (\dot{m}_j V_{j1} + p_{j1} A_{j1}) * \cos(\theta_1 - \alpha) - \gamma(\dot{m}_j V_{j2} + p_{j2} A_{j2}) * \cos(\theta_2 + \alpha) \end{aligned} \quad (3)$$

where γ is the suction coefficient. If $\gamma = 1$, the suction is on. If $\gamma = 0$, the suction is off and the co-flow jet has injection only. The θ is the angle between the slot surface and the line normal to the airfoil chord(see Fig.3). For the CFJ0025-065-196 airfoil[9] analyzed in this paper, $\theta_1 = 25.86^\circ$, $\theta_2 = 14.31^\circ$, α is the angle of attack, V_j is the jet velocity, p_j is the jet static pressure, \dot{m}_j is the jet mass flow rate, A_j is the jet slot area.

The total drag, which is the one measured by the wind tunnel balance, is the summation of the airfoil surface drag and the reaction force in drag direction generated by the injection and suction ducts. Based on the Newton's 3rd law that a force and its reaction force have the same magnitude and opposite direction, the drag D is then:

$$D = -(R_x + F_{x_{cfj}}) = R'_x - F_{x_{cfj}} \quad (4)$$

R'_x is the CFJ airfoil surface pressure and shear stress integral in x-direction.

$$R'_x = -R_x \quad (5)$$

Substituting Eq.(2) and (3) into Eq.(4), then the total drag is:

$$D = R'_x - F_{x_{cfj}} = \int_i^a \rho V_\infty \cdot dy \cdot V_\infty - \int_h^b \rho V_e \cdot dy \cdot V_e \quad (6)$$

For CFJ airfoil, the injection and suction have the same mass flow rate. Hence, the mass conservation gives:

$$\dot{m}_{j1} = \dot{m}_{j2} \quad (7)$$

and

$$\int_i^a \rho V_\infty \cdot dy = \int_h^b \rho V_e \cdot dy \quad (8)$$

Equation (6) then becomes:

$$D = R'_x - F_{x_{cfj}} = \int_h^b \rho V_e (V_\infty - V_e) dy \quad (9)$$

or

$$C_D = C_{Drake} \quad (10)$$

Some conclusions can be drawn from the equations above: 1) For a CFJ airfoil, the total drag is the drag measured by the wind tunnel balance, and is equal to the drag calculated by the wake rake measurement. This is the same as for a conventional airfoil with no flow control or an airfoil using flow control with zero net mass flow rate.; 2) The injection has the effect of reducing drag due to the jet thrust.; 3)The suction has the effect of increasing drag.

The lift measured by the wind tunnel balance is:

$$L = R'_y - F_{y_{cfj}} \quad (11)$$

Where R'_y is the y-direction component of the surface pressure and shear stress integral, which is primarily induced by the circulation. $F_{y_{cfj}}$ is the jet ducts reaction force component in y-direction.

$$\begin{aligned} F_{y_{cfj}} &= (\dot{m}_{j1}v_{j1} + (p_{j1}A_{j1})_y) - \gamma(\dot{m}_{j2}v_{j2} + (p_{j2}A_{j2})_y) \\ &= (\dot{m}_jV_{j1} + p_{j1}A_{j1}) * \sin(\theta_1 - \alpha) + \gamma(\dot{m}_jV_{j2} + p_{j2}A_{j2}) * \sin(\theta_2 + \alpha) \end{aligned} \quad (12)$$

Eq.(11) and (12) indicate that: 1) the injection has the effect of reducing lift when $v_{j1} > 0$, increasing lift when $v_{j1} < 0$.; 2)The suction almost always has the effect of decreasing lift.

3.2 Airfoil with Jet Injection Only

A sketch of a injection only airfoil integrated with an aircraft engine is shown in Fig.2. The jet mass flow is sucked form engine inlet from freestream and injected on the airfoil.

In a wind tunnel test, when an airfoil has injection jet only such as the CC airfoil, the jet mass flow is usually drawn from outside of the wind tunnel. The jet mass flow is added into the total wind tunnel exit mass flow. The mass conservation hence gives:

$$\int_i^a \rho V_\infty \cdot dy = \int_h^b \rho V_e \cdot dy - \dot{m}_j \quad (13)$$

Since there is no suction, the measured drag in a wind tunnel test based on eq. (6) is:

$$D_{windtunnel} = R'_x - (\dot{m}_j u_j + (p_j A_j)_x) = R'_x - (\dot{m}_j V_{j1} + p_{j1} A_{j1}) * \cos(\theta_1 - \alpha) = \int_h^b \rho V_e (V_\infty - V_e) dy - \dot{m}_j V_\infty \quad (14)$$

Or

$$C_{D_{windtunnel}} = C_{Drake} - C_\mu \frac{V_\infty}{V_j} \quad (15)$$

where C_μ is defined as:

$$C_\mu = \frac{\dot{m}_j V_j}{0.5 \rho_\infty U_\infty^2 S} \quad (16)$$

That is: for an airfoil with jet blowing only, the drag measured by the balance in a wind tunnel is equal to the drag calculated based on the wake rake measurement minus $\dot{m}_j V_\infty$. This is the same conclusion as that given in [17] and adopted in [18].

However, in reality, when the airfoil with jet blowing only is used in an aircraft, there must be an air flow source for the blowing. Usually, the engine sucks in the air from the freestream and is blown on the wing surface as shown in Fig. 2.

Assume that the wing blowing airflow source is from the engine inlet, the actual drag that the airfoil will experience can be still determined by Eq. (6). The difference is that the suction parameters will be those at engine inlet. The actual drag with the suction effect is also often called equivalent drag [18].

$$D_{equiv} = R'_x - (\dot{m}_j u_j + (p_j A_j)_x) + \dot{m}_j V_{ei} + p_{ei} A_{j_{ei}} \quad (17)$$

The subscript ei stands for engine inlet. Based on Eq.(14), the equivalent drag is:

$$D_{equiv} = D_{windtunnel} + \dot{m}_j V_{ei} + p_{ei} A_{j_{ei}} \quad (18)$$

$A_{j_{ei}}$ is the captured area to draw the blown jet mass flow from freestream. The drag due to the term $\dot{m}_j V_{ei}$ is the ram drag. The drag due to the term $p_{ei} A_{j_{ei}}$ is the captured area drag.

Based on mass conservation,

$$\rho_{ei} V_{ei} A_{j_{ei}} = \dot{m}_j \quad (19)$$

$$p_{ei} A_{j_{ei}} = \frac{\dot{m}_j V_{ei}}{\gamma M_{ei}^2} \quad (20)$$

Then Eq.(18) becomes:

$$\begin{aligned} C_{D_{equiv}} &= C_{D_{windtunnel}} + C_\mu \frac{V_{ei}}{V_j} + C_\mu \frac{V_{ei}}{V_j \gamma M_{ei}^2} \\ &= C_{D_{windtunnel}} + C_\mu \frac{V_{ei}}{V_j} \left(1 + \frac{1}{\gamma M_{ei}^2}\right) \end{aligned} \quad (21)$$

Eq.(21) indicates that, when the Mach number at engine inlet is increased, the ram drag is also increased due to the higher velocity, and the captured area drag is decreased due to the reduced captured area for the jet. The captured area drag is significantly larger than the ram drag if the flow at engine inlet is subsonic. During a flight mission, the flow parameters at the engine inlet may or may be equal to the freestream parameters. For example, at the starting point to take off, the freestream velocity is zero, but the velocity at the engine inlet is far greater than zero to satisfy the engine mass flow requirement to generate the required thrust. During a flight mission, when the mass flow rate required by the engine is equal to the mass flow rate captured by the straight flow tube going into the engine inlet, the freestream flow parameters will be equal to the flow parameters at engine inlet. The drag increase for the airfoil with injection only due to the ram and captured area drag can be also considered as the loss of thrust[?].

If assume $V_{ei} = V_\infty$, based on Eq.(15), we have:

$$C_{Dequiv} = C_{Drake} + C_\mu \frac{V_{ei}}{V_j \gamma M_{ei}^2} \quad (22)$$

The lift for the airfoil with injection only is:

$$L = R'_y - (\dot{m}_{j1} v_{j1} + (p_{j1} A_{j1})_y) = R'_y - (\dot{m}_j V_{j1} + p_{j1} A_{j1}) * \sin(\theta_1 - \alpha) \quad (23)$$

The jet suction from the freestream has no component in y-direction. Hence the lift above is the same as the lift measured by the wind tunnel balance.

The equivalent drag formulation used in [18, 19] is different from the one derived in this paper. The assumption used in [18, 19] is that the jet is taken from a large reservoir. As a reference, the formulation is given below[18]:

$$C_{Dequiv} = C_{Dwindtunnel} + C_\mu \frac{V_\infty}{V_j} + C_\mu \frac{V_j}{2V_\infty} \quad (24)$$

Using Eq.(15),

$$C_{Dequiv} = C_{Drake} + C_\mu \frac{V_j}{2V_\infty} \quad (25)$$

4 Jet Effect on Airfoil Performance

Compare Eq.(9) and (14), one of the important differences between the CFJ airfoil and the airfoil with injection only (e.g. a CC airfoil) is: For the airfoil with injection only, the drag actually acted on the aircraft, the equivalent drag, could be significantly larger than the drag measured by the wind tunnel balance because of the ram and captured area drag when the jet is drawn from the freestream through engine inlet. For a CFJ airfoil, the drag measured by the wind tunnel balance is the actual 2D drag that the aircraft will be experienced. The CFJ airfoil does not have the ram drag and captured area drag.

The reason for above difference is that for a 2D CFJ airfoil, the mass conservation is satisfied by recirculating the jet. The jet injection and suction effect is included in the measured lift and drag in a wind tunnel. For a 2D injection only airfoil such as a CC airfoil, the jet mass flow is not conserved since there is no jet flow source inside the airfoil. However, this does not prevent the measurement of a 2D airfoil with injection only in a wind tunnel since the jet flow can be drawn into the airfoil from the side, which is perpendicular to the streamwise plane. The suction hence will have no effect on the drag and lift.

For a CFJ airfoil, both the injection and suction occur on the suction surface of the airfoil. Compared with an airfoil with injection only, the CFJ airfoil will have the jet attached more strongly due to the suction. This will induce a stronger circulation and have a higher stall AoA than the airfoil with injection only. The distance between the injection and suction provides an intensive mixing process. The adverse pressure gradient also enhances the mixing, which fills the wake and reduces drag. The shallower the wake profile, the smaller the drag. If the wake has

reversed velocity deficit, a thrust is generated. The CFJ airfoil will usually have a significantly lower drag than the airfoil with injection only due to the stronger mixing.

The power required to pump the co-flow jet for CFJ airfoil based on Eq. (3) is:

$$P_{cfj} = V_{\infty} F_{x_{cfj}} = V_{\infty} [(\dot{m}_j V_{j1} + p_{j1} A_{j1}) * \cos(\theta_1 - \alpha) - (\dot{m}_j V_{j2} + p_{j2} A_{j2}) * \cos(\theta_2 + \alpha)] \quad (26)$$

The power required to pump the jet flow for the airfoil with injection only is:

$$P_{inj \ only} = V_{\infty} F_{x_{inj \ only}} = V_{\infty} [(\dot{m}_j V_{j1} + p_{j1} A_{j1}) * \cos(\theta_1 - \alpha) - (\dot{m}_j V_{ei} + p_{ei} A_{j_{ei}})] \quad (27)$$

The CFD results to be seen later indicates that the $P_{inj \ only}$ is significantly greater than P_{cfj} .

5 CFD Solver

The Fluent CFD software is used in this research to calculate the 2D and 3D CFJ airfoil flows. The governing equations are the Reynolds averaged 3D compressible Navier-Stokes (RANS) equations. The pressure based second order upwind scheme is used to evaluate the inviscid flux and central differencing is used for the viscous terms. The $k - \epsilon$ turbulence model with integration to the wall and pressure gradient effect is employed. The y_1^+ is in the order of 1. The $k - \epsilon$ model is selected due to its capability of taking into account of turbulent boundary layer history effect by solving the complete transport equations of k and ϵ , and the $k - \epsilon$ model is more capable than algebraic models to predict the separated flows, which occur when the airfoil stalls at high AoA.

The full turbulent boundary layer assumption is used and is consistent with the tripped boundary layer in the experiments. Mesh refinement study is conducted for a few selected points to ensure that the solutions are mesh size independent. Since the CFD solutions are obtained from the steady state calculations based on RANS model, the unsteady details of the shear layer mixing entrainment and large coherent vortex structures are not able to be captured.

The wind tunnel walls are included in the CFD simulation to consider the wind tunnel wall effect. The total pressure and total temperature are given at the wind tunnel inlet as the boundary conditions. The static pressure at wind tunnel exit is iterated to make the wind tunnel inlet Mach number match the experimental value. The total pressure and total temperature are also given at the injection duct inlet as the boundary conditions. The injection total pressure is iterated to match the experimental momentum coefficient. The static pressure at the suction duct entrance is iterated to match the injection jet mass flow rate.

As mentioned above, several layers iterations are needed to achieve a converged CFJ airfoil solution at a certain AoA. The calculation is thus very CPU intensive, in particular for 3D cases. The 2D CFJ airfoil calculation is therefore very desirable. The control volume analysis in this paper not only gives an insight of the CFJ airfoil working principle, but also provides the formulation to calculate the lift and drag generated by the jet ducts.

6 Results and Discussion

6.1 Geometry

Fig.4 shows the baseline airfoil, NACA0025, and the CFJ airfoil. The NACA0025 airfoil was selected as the baseline airfoil due to its large thickness to facilitate implementation of co-flow jet, internal ducts, and instrumentation. The chord length of the airfoil is 0.1527m and the span is 0.3m. The co-flow jet airfoils are named using the following convention: CFJ4dig-INJ-SUC, where 4dig is the same as NACA 4 digit convention, INJ is replaced by the percentage of the injection slot size to the chord length and SUC is replaced by the percentage of the suction slot size to the chord length. For example, the CFJ0025-065-196 airfoil has the injection slot height of 0.65% of the chord and the suction slot height of 1.96% of the chord. The suction surface shape is a downward translation of the portion of the original suction surface between the injection and suction slot. The injection and suction slot are located at 7.11% and 83.18% of the chord from the leading edge. The slot faces are normal to the suction surface to make the jet tangential to main flow. In the experiment, the high pressure flow is injected into the high pressure cavity and then goes through a metallic foam to make the injection jet uniform. The CFD simulations take the downstream interface of the foam as the injection inlet.

6.2 CFJ Airfoil with both injection and suction

Figure 5 is the zoomed 2D mesh near the CFJ0025-065-196 airfoil. The structured mesh is used around the airfoil and unstructured mesh is used in the region away from the airfoil where the flow gradient is small. The total number of cells is 170k. The freestream Mach number is about 0.1 and the Reynolds number based on chord is 380k. The flow is assumed normal to the injection duct inlet. The suction duct is only simulated with an entrance opening since the flow inside the suction duct has little effect on the flow outside of the suction duct. Simulation of the injection duct gives a more realistic injection mixing effect when the jet enters into the mainflow. Figure 6 is the Mach number contours and streamlines of the CFJ0025-065-196 airfoil at $AoA=39^\circ$. The flow is attached and is consistent with experiment[9].

Figure 7 is the computed lift coefficient compared with the experiment. The two solid lines with solid symbols are the experimental results of the CFJ airfoil and the baseline airfoil. The CFJ airfoil has increased maximum lift by 220% and stall margin by 153%. The predicted baseline airfoil lift (open triangle symbols) agrees fairly well with the experiment (solid triangle symbols), except that the stall AoA is about 3 degree higher than the experiment.

The open square symbol is the lift coefficient calculated by the surface integral of pressure and shear stress. This is the lift generated primarily by circulation, which is the R'_y given in eq.(11) and is expected to be higher than the measured lift. The open diamond symbols are the lift contribution made by the injection duct reaction force, the first item of Eq.(12). It can be seen that the injection jet does not have a large effect on lift. When the suction effect is added, the final lift is reduced as shown by the open circle symbols. The suction has more effect on the lift. The lift with the jet ducts reaction force is given as the circle based on eq.(11). Obviously, the computed lift agrees fairly well with the experiment up to $AoA=20^\circ$. When the AoA is greater than 20° , the computation under-predicts the lift significantly. The large discrepancy may be due to the inherent unsteadiness of the mixing process at high AoA under large adverse pressure gradient. The RANS model used in this paper may be not adequate to capture the unsteady mixing process, which could have large

vortex structure such as the coherent vortices due to the jet dissimilarity and Görtler vortices due to the surface curvature. The very bottom curve with triangle symbol in Fig. 7 is the calculated total lift contribution generated by the jet ducts based on Eq.(12). The lift reduction is significant and is mainly made by the suction jet.

Figure 8 is the computed drag coefficient compared with the experiment. The two bold lines are the measured drag coefficient of the CFJ airfoil and the baseline airfoil. The CFJ airfoil has lower drag than the baseline airfoil before the baseline airfoil stalls. In the region of zero angle of attack, the CFJ airfoil has negative drag, that is thrust. The CFD slightly under-predicts the baseline airfoil drag coefficient when $\text{AoA} \leq 10^\circ$. The predicted drag coefficient remains flat at high AoA for the baseline airfoil, whereas the measured baseline airfoil drag coefficient increases at high AoA. The discrepancy of the baseline airfoil drag prediction is hence increased at high AoA.

The open square symbol is the drag coefficient determined by the surface integral of pressure and shear stress, the R'_x in Eq. (4). It is largely below the measured drag and has negative value up to nearly $\text{AoA}=50^\circ$. The negative drag is primarily due to the strong leading edge suction, which results in a thrust force due to the pressure integral. The injection further reduces the drag due to the jet momentum as shown by the open diamond symbols and is calculated based on Eq.(3) and (4). When the suction duct reaction force is added, the drag is brought very close to the measured drag as shown by the open circle symbols. This shows that the control volume analysis indeed gives a good quantitative correction of the drag. Similar to the lift prediction, the CFJ airfoil drag is predicted quite well at low AOA. At high AoA, the CFJ airfoil drag prediction is similar to the baseline case and is fairly flat most probably due to the inadequate turbulence simulation by RANS model. The dash line curve with the open triangle symbols is the total force due to the jet ducts calculated based on Eq.(3). It can be seen that the jet ducts have a significant contribution to the drag.

To validate the ducts reaction force computed based on Eq. (3) and (12), a 3D case with the airfoil, wind tunnel walls and the experimental injection and suction ducts are simulated at zero angle of attack. Figure 10 shows the 3D mesh and Fig. 11 shows the 3D streamlines released from the injection duct, which indicates that the flow field has a good two-dimensionality. For the surface force integral calculation of the injection duct, the duct inlet is treated as a fictitious wall so that the pressure on the wall can be counted as in the experiment. The total 3D resultant force generated by the ducts can then be obtained. The 2D total drag and lift can thus be calculated based on Eq.(4) and (11). However, the $F_{x_{cfj}}$ and $F_{x_{cfj}}$ are determined by the 3D duct surface integral force instead of Eq.(3) and (12) for validation. An assumption is made that the resultant force generated by the ducts has constant magnitude at different AoA and is always along the chordwise direction. The calculated lift and drag coefficients are shown in Fig.7 and 8 as the dot lines with open right-triangle symbols. They agree amazingly well with the results using the 2D control volume correction.

The 3D results support two conclusions: 1) the results of the 2D control volume analysis provide accurate duct reaction forces for the lift and drag; 2) The assumption that the ducts resultant force has constant magnitude at different AoA and is along the chordwise direction is reasonable. The rationale for this assumption is that the duct internal force is not affected much by the airfoil main flow field at different AoA.

6.3 Suction Effect

To compare the performance of a CFJ airfoil and an airfoil with injection only, the CFJ0025-065-000 airfoil is created with no suction slot. The last 3 digit 000 means there is no suction slot. The injection slot is exactly the same. The suction surface has the same shape as that of the baseline NACA0025 airfoil suction surface. The injection momentum coefficient is the same as that of the CFJ0025-065-196 airfoil for comparison purpose. The results at $AoA=20^\circ$ are used for comparison.

Figure 12 and 13 are the Mach contours of the CFJ0025-065-000 airfoil and CFJ0025-065-196 airfoil and they give the following observations: 1) The CFJ0025-065-000 airfoil has a large wake region with low momentum. The CFJ0025-065-196 airfoil hardly has a wake. This indicates that the CFJ airfoil with both injection and suction has stronger mixing than the airfoil with injection only. The main flow is more energized by the jet with both injection and suction. 2) The stagnation point of the CFJ0025-065-196 airfoil is more downstream than that of the CFJ0025-065-000 airfoil. This indicates that the circulation induced by the CFJ airfoil is greater than that of the airfoil with injection only. The higher circulation also yields higher leading edge peak Mach number.

Figure 14 is the wake profiles of the CFJ0025-065-196 airfoil and CFJ0025-065-000 airfoil. Even though both airfoils have the same injection jet location and jet strength, the CFJ0025-065-196 airfoil has reversed velocity deficit, whereas the CFJ0025-065-000 airfoil has a deep wake. This means that the suction enhances the mixing and fills the wake more than the airfoil without suction. There is more energy transferring between the jet and the mainflow when both injection and suction are used.

Figure 15 is the surface isentropic Mach number for CFJ0025-065-196 airfoil and CFJ0025-065-000 airfoil. It can be seen that the surface loading, or the circulation, of the CFJ0025-065-196 airfoil is much larger than that of the CFJ0025-065-000 airfoil. The leading edge suction peak Mach number of the CFJ0025-065-196 airfoil is higher and the stagnation point is more downstream. It can be seen that the injection location is located downstream of the peak Mach number in order to make use of the adverse pressure gradient to enhance mixing.

Tables 1 - 3 compare the performance of the CFJ0025-065-196 (with injection and suction) and CFJ0025-065-000 (with injection only) airfoil. The flow parameters at the engine inlet are assumed to be equal to the freestream flow parameters.

Table 1 compares the CFD lift coefficients and their breakdowns for the CFJ0025-065-196 and CFJ0025-065-000 airfoil. The momentum coefficients of the two airfoil are about the same, with that of the CFJ0025-065-000 airfoil about 4% higher. The CFD solver is the same for the two simulations and the mesh sizes are about the same. Table 1 indicates that the lift coefficient of the CFJ0025-065-196 airfoil is 42% higher than that of the CFJ0025-065-000 airfoil. The primary contribution is from the lift generated by circulation, which is 115% higher than that of the CFJ0025-065-000 airfoil. The injection jet generates about the same lift reduction for both airfoil. The suction generates a lift reduction for the CFJ0025-065-196 airfoil. For CFJ0025-065-000 airfoil, the suction is from the freestream and hence has no lift component.

Table 2 compares the drag coefficients and their breakdowns for the CFJ0025-065-196 and CFJ0025-065-000 airfoil based on the same solutions used for the lift comparison. Table 2 indicates that the drag coefficients of the CFJ0025-065-196 airfoil is lower than that of the CFJ0025-065-000 airfoil. For CFJ0025-065-196 airfoil, the surface force integral generates a large thrust. This is because that the high circulation induces a strong leading edge suction with low pressure, which results in a forward thrust. On the contrary, for CFJ0025-065-000 airfoil, the surface force integral

generates a large drag as a conventional airfoil. The injection reduces drag for both airfoils due to the injection jet thrust. The suction induces a large drag. If the drags of the two airfoils are considered as not too much different, the equivalent drag of the CFJ0025-065-000 airfoil is significantly larger than that of the CFJ0025-065-196 airfoil. The equivalent drag is the drag that the designers should actually use for an aircraft design. For the CFJ0025-065-000 airfoil, the suction drag calculated by the formulation given in the present paper is significantly larger than that calculated by the equation given in [18]. However, even based on the formulation given in [18], the equivalent drag of the airfoil with injection only is much larger than that of the CFJ airfoil.

The power required to pump the jet for the CFJ0025-065-196 and CFJ0025-065-000 airfoils are calculated based on Eqs.(26) and (27) and is given in Table 3. The power required to pump the CFJ0025-065-000 airfoil with injection only is 2.4 times that required to pump the CFJ0025-065-196 airfoil.

In conclusion, a suction process of the jet is necessary for any flow control method as long as the flow control needs an injection. This is governed by the law of mass conservation. The question is: where is more beneficial to let the suction occur, on the airfoil such as the CFJ airfoil or on the engine? The analysis above indicates that the streamwise suction of the CFJ airfoil enhance mixing, induce large circulation, and reduce drag. The drag measured in the wind tunnel is the drag that will be acted on an aircraft(excluding induce drag). In other words, the performance penalty of a CFJ airfoil due to the suction is already counted and the equivalent drag is the same as the drag measured in a wind tunnel. The penalty to the drag and lift generated by the suction momentum is offset by the higher circulation and stronger leading edge suction generated by both the injection and suction.

Airfoil	C_μ	C_L	R'_y	F_y inj.	F_y suc.
CFJ0025-065-196	0.208	2.36	3.78	-0.095	-1.33
CFJ0025-065-000	0.217	1.66	1.76	-0.1	0

Table 1: Comparison of lift coefficient and its breakdowns for the two CFJ airfoils at AoA=20°.

Airfoil	C_D	R'_x	F_x inj.	F_x suc.	C_D equiv
CFJ0025-065-196	-0.017	-1.03	-0.93	1.94	-0.017
CFJ0025-065-000	0.17	1.14	-0.97	3.43	3.6 (present), 0.7(Jones[18])

Table 2: Comparison of drag coefficient and its breakdowns for the two CFJ airfoils at AoA=20°..

Airfoil	Power Required
CFJ0025-065-196	1
CFJ0025-065-000	2.4

Table 3: Comparison of the power required to pump the jet for the two CFJ airfoils at AoA=20°..

7 Conclusions

The control volume analysis provides the lift and drag breakdowns of a CFJ airfoil contributed by its surface force integral and the reaction forces generated by the jet ducts. These formulations also provides the necessary duct reaction forces to be included for 2D CFJ airfoil calculation. The lift and drag calculated by CFD using $-k - \epsilon$ turbulence model are compared well with the experiment when the AoA is less than 20° . At high AoA, both the lift and drag are significantly under predicted. The large discrepancy at high AoA may be primarily due to the inadequacy of a RANS turbulence model to simulate the unsteady jet mixing process. The duct reaction forces are also validated by a 3D CFD calculation of the complete airfoil with jet ducts and wind tunnel wall.

A suction process of the jet is necessary for all flow control methods as long as they use flow injection. This is the result of the mass conservation law. The comparative study between a CFJ airfoil with injection and suction and a airfoil with the injection only is conducted. The study indicates that the suction occurring on the airfoil suction surface such as the CFJ airfoil is more beneficial than the suction occurring through the engine inlet such as the airfoil with injection only. For the airfoil with injection only, the drag actually acted on the aircraft, the equivalent drag, is significantly larger than the drag measured by the wind tunnel balance because of the ram and captured area drag when the jet is drawn from the freestream. For a CFJ airfoil, the drag measured by the wind tunnel balance is the actual 2D drag that the aircraft will be experienced. The CFJ airfoil does not have the ram drag and captured area drag. For a CFJ airfoil, the suction penalty is offset by the significant circulation enhancement. The CFJ airfoil with both injection and suction yields stronger mixing, larger circulation, more filled wake , higher stall angle of attack, less drag, and more efficient energy expenditure.

References

- [1] W. L. I. Sellers, B. A. Singer, and L. D. Leavitt, "Aerodynamics for Revolutionary Air Vehicles." AIAA 2004-3785, June 2003.
- [2] M. Gad-el Hak, "Flow Control: The Future ," *Journal of Aircraft*, vol. 38, pp. 402–418, 2001.
- [3] M. Gad-el Hak, *Flow Control, Passive, Active, and Reactive Flow Management*. Cambridge University Press, 2000.
- [4] S. Anders, W. L. Sellers, and A. Washburn, "Active Flow Control Activities at NASA Langley." AIAA 2004-2623, June 2004.
- [5] C. P. Tilmann, R. L. Kimmel, G. Addington, and J. H. Myatt, "Flow Control Research and Application at the AFRL's Air Vehicles Directorate." AIAA 2004-2622, June 2004.
- [6] D. Miller, , and G. Addington, "Aerodynamic Flowfield Control Technologies for Highly Integrated Airframe Propulsion Flowpaths." AIAA 2004-2625, June 2004.
- [7] V. Kibens and W. W. Bower, "An Overview of Active Flow Control Applications at The Boeing Company." AIAA 2004-2624, June 2004.
- [8] G.-C. Zha and D. C. Paxton, "A Novel Flow Control Method for Airfoil Performance Enhancement Using Co-Flow Jet." *Applications of Circulation Control Technologies*, Progress in

- Astronautics and Aeronautics, AIAA Book Series, Editors: Joslin, R. D. and Jones, G.S., to be published in 2006.
- [9] G.-C. Zha, B. Carroll, C. Paxton, A. Conley, and A. Wells, “High Performance Airfoil with Co-Flow Jet Flow Control.” AIAA-Paper-2005-1260, Jan. 2005, submitted for publication in AIAA Journal.
 - [10] G.-C. Zha, C. Paxton, A. Conley, A. Wells, and B. Carroll, “Effect of Injection Slot Size on High Performance Co-Flow Jet Airfoil.” Submitted to AIAA Journal of Aircraft, April 2005.
 - [11] G.-C. Zha and C. Paxton, “A Novel Airfoil Circulation Augment Flow Control Method Using Co-Flow Jet.” NASA/CP-2005-213509, June 2005; AIAA Paper 2004-2208, June 2004.
 - [12] R. J. Englar, “Circulation Control for High Lift and Drag Generation on STOL Aircraft,” *Journal of Aircraft*, vol. 12, pp. 457–463, 1975.
 - [13] R. J. Englar, L. A. Trobaugh, and R. Hemmersly, “STOL Potential of the Circulation Control Wing for High-Performance Aircraft,” *Journal of Aircraft*, vol. 14, pp. 175–181, 1978.
 - [14] Y. Liu, L. N. Sankar, R. J. Englar, K. K. Ahuja, and R. Gaeta, “Computational Evaluation of the Steady and Pulsed Jet Effects on the Performance of a Circulation Control Wing Section.” AIAA Paper 2004-0056, 42nd AIAA Aerospace Sciences Meeting and Exhibit, Reno, Nevada 5 - 8 Jan 2004.
 - [15] I. Wygnanski, “The Variables Affecting The Control Separation by Periodic Excitation.” AIAA 2004-2625, June 2004.
 - [16] E. M. Greitzer, C. S. Tan, and M. B. Graf, *Internal Flow*. Cambridge University Press, 2004.
 - [17] R.-J. Jones, “A Proposed Method of Circulation Control.” University of Cambridge Ph.D. Thesis, June 1969.
 - [18] G. S. Jones, “Pneumatic Flap Performance for a 2D Circulation Control Airfoil, Steady & Pulsed.” NASA/CP-2005-213509, June 2005, and *Applications of Circulation Control Technologies*, Progress in Astronautics and Aeronautics, AIAA Book Series, Editors: Joslin, R. D. and Jones, G.S., to be published in 2006.
 - [19] M. Wilson and C. von Kerczek, “An Inventory of Some Force Procedure for Use in Marine Vehicle Control.” DTNSRDC-791097, Nov, 1979.

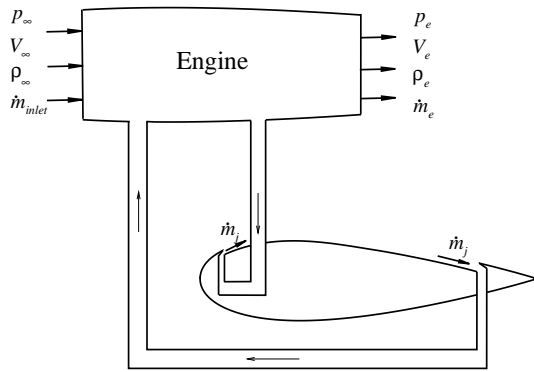


Figure 1: Sketch of a CFJ airfoil integrated with a propulsion system.

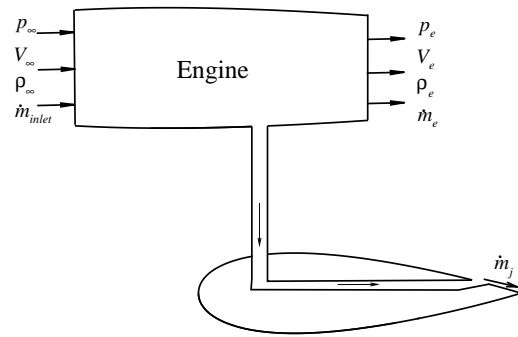


Figure 2: Sketch of an injection airfoil integrated with a propulsion system.

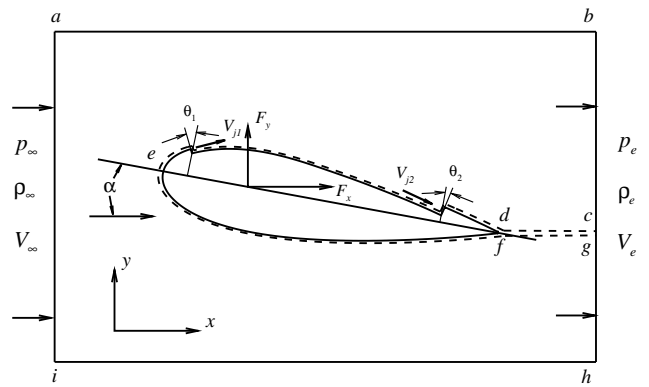


Figure 3: The control volume for a CFJ airfoil.

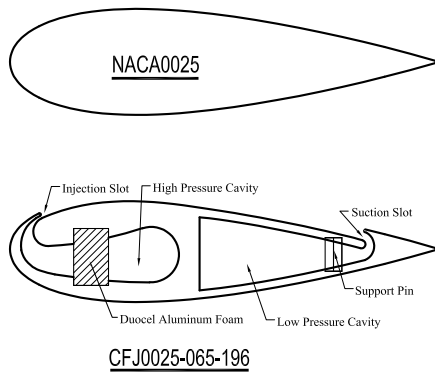


Figure 4: Airfoil section of the baseline airfoil of NACA0025 and CFJ airfoil CFJ0025-065-196.

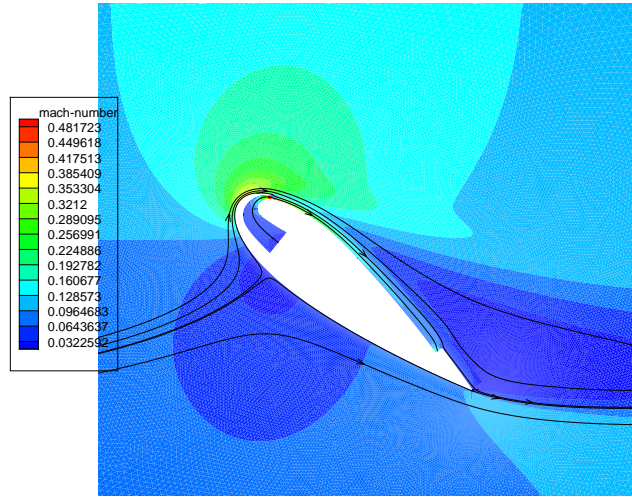


Figure 6: Computed Mach number contours with streamlines for CFJ0025-065-196 airfoil at $AoA=39^\circ$.

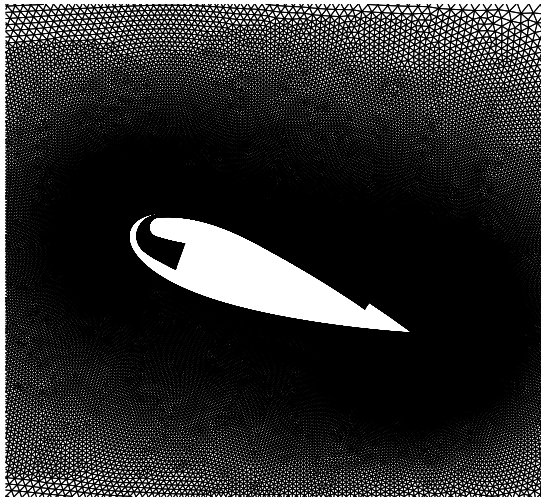


Figure 5: 2D mesh for CFD calculation of the CFJ0025-065-196 airfoil.

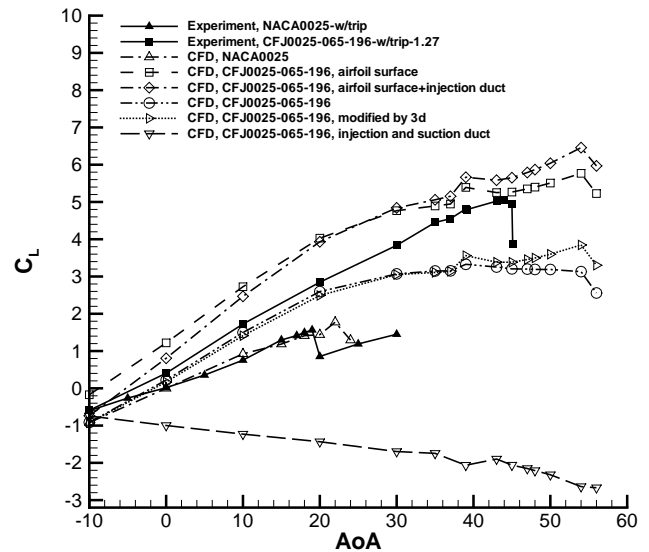


Figure 7: Computed lift coefficient compared with experiment at different AoA .

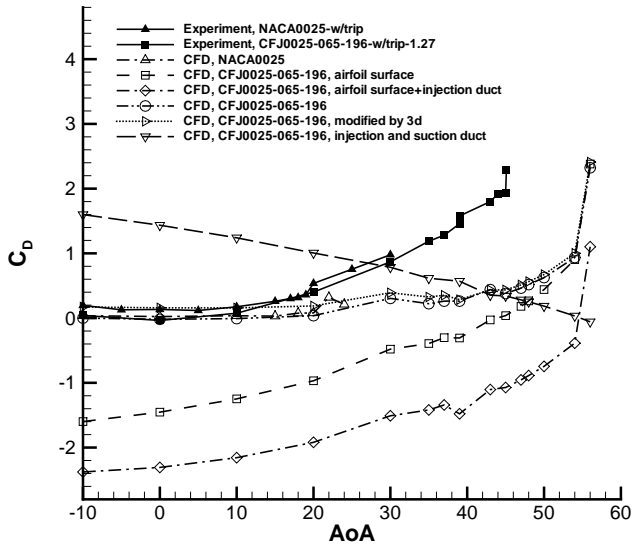


Figure 8: Computed drag coefficient compared with experiment at different AoA.

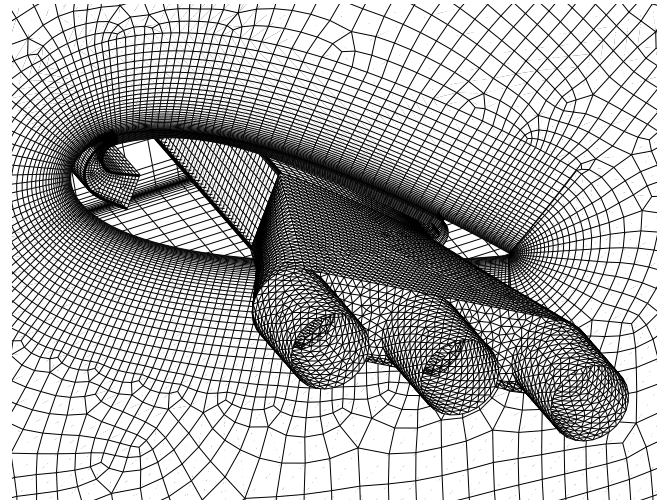


Figure 10: 3D mesh for CFD calculation of the CFJ0025-065-196 airfoil with injection and suction ducts.

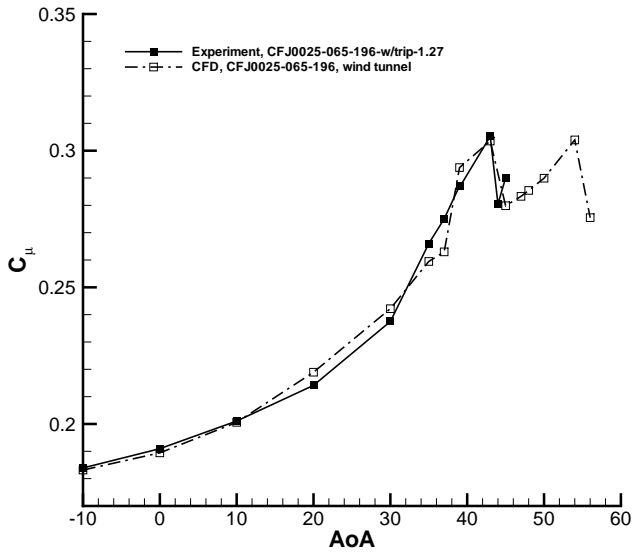


Figure 9: Computed momentum coefficient compared with experiment at different AoA.

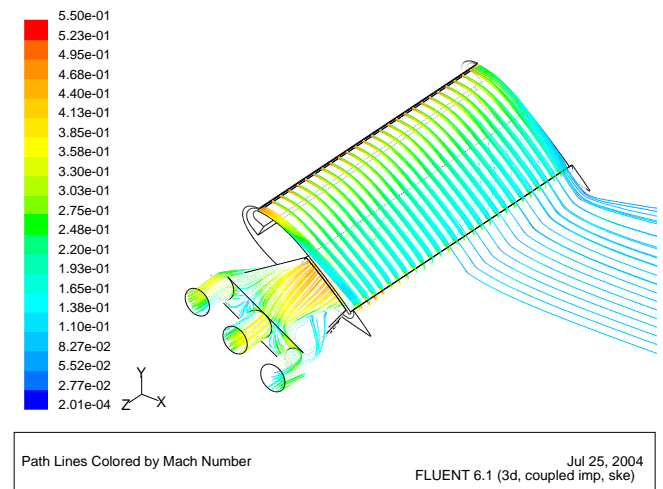


Figure 11: Streamlines released from the injection jet of the 3D calculation.

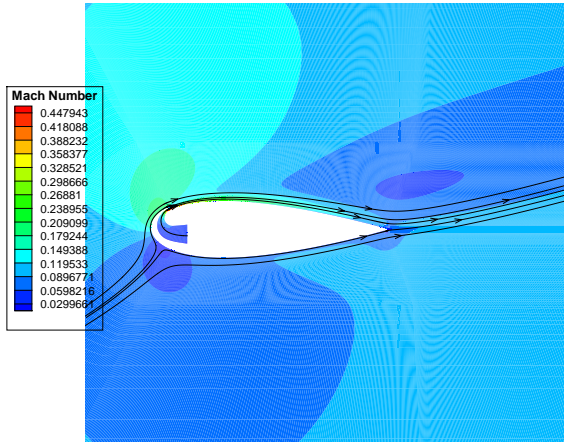


Figure 12: Mach number contours with streamlines for CFJ0025-065-000 airfoil with injection only at $AoA=20^\circ$.

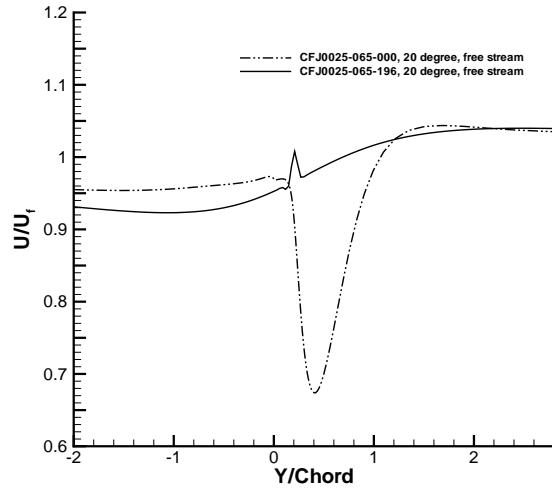


Figure 14: Wake profiles of the CFJ airfoil and the airfoil with injection only.

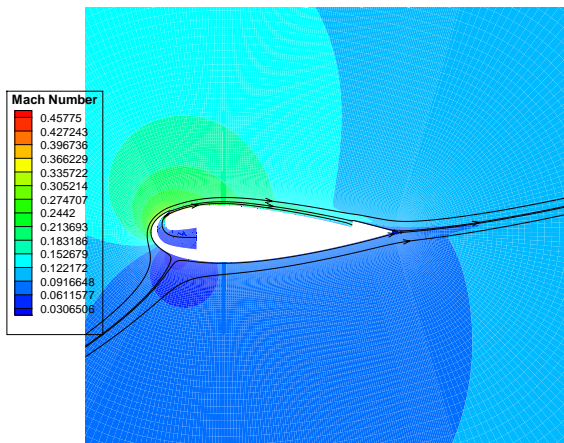


Figure 13: Mach number contours with streamlines for CFJ0025-065-196 airfoil at $AoA=20^\circ$.

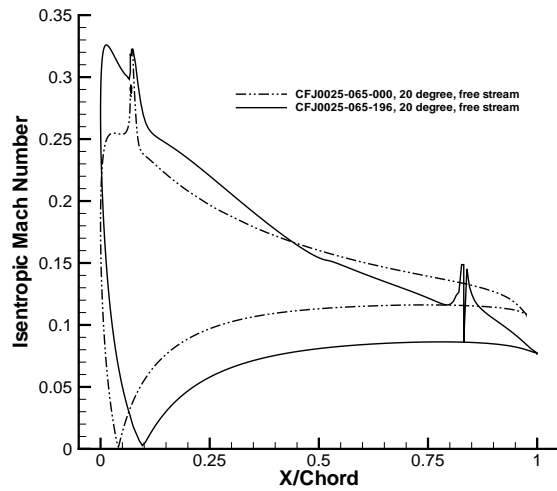


Figure 15: Wake profiles of the CFJ airfoil and the airfoil with injection only.